# Monte Carlo tuning for the BESIII time-of-flight system*

ZHANG Xiao-Jie(张晓杰)[1)] SUN Sheng-Sen(孙胜森)[2)] DENG Zi-Yan(邓子艳)
LIU Yong(刘勇) LIU Huai-Min(刘怀民) WANG Yi-Fang(王贻芳)
Institute of High Energy Physics, Chinese Academy of Sciences, Beijing 100049, China

**Abstract:** Using experimental data, Monte Carlo tuning is implemented for performance parameters associated with the scintillation counters and readout electronics of the BESIII time-of-flight (TOF) system, as part of the full simulation model. The implementation of the tuning is described for simulations designed to reproduce the performance of a number of TOF system parameters, including pulse height, hit efficiency, time resolution, dead channels and background. In addition, comparisons with experimental data are presented.

**Key words:** time-of-fight(TOF) detector, Monte Carlo tuning, detector simulation

**PACS:** 29.40.Mc, 29.85.Fj **DOI:** 10.1088/1674-1137/38/6/066204

## 1 Introduction

The Beijing Spectrometer (BESIII) [1, 2] located at the upgraded Beijing Electron Positron Collider (BEPC II) [3] is a high precision general purpose detector that is designed to study physics in the τ-charm energy region. One of the sub-detectors, the time-of-flight (TOF) system, which is based on plastic scintillation counters, is a powerful tool for particle identification (PID) and can provide fast trigger signals.

Reliable Monte Carlo (MC) simulation plays an important role in understanding the detector system and in minimizing systematic uncertainties for physics analysis. A full Monte Carlo model based on GEANT4 [4, 5] has been developed to simulate the performance of the BESIII time-of-flight system. The precise simulation of physics processes, including optical photon propagation in the TOF counters, electronic processes in the discriminator, and the effect of dead channels and background, depends on the Monte Carlo tuning of scintillator and electronics performance parameters, which are determined using real $e^+e^-$ collision data.

In this paper, the Monte Carlo tuning for the BESIII TOF detector simulation is described. The TOF system in the BESIII detector and the TOF simulation procedure are briefly introduced in Sections 2 and 3, respectively. The tuning of the pulse height and hit efficiency simulation is described in Sections 4.1 to 4.3. The timing tuning is discussed in Section 4.4, and the simulation of dead channels and background is introduced in Section 4.5. The MC tuning results compared with real data are also shown.

## 2 The BESIII detector TOF system

The BESIII detector is configured around a 1 T superconducting solenoid magnet (SSM), the main spectrometer components are: the multilayer drift chamber (MDC) surrounding the beryllium beam pipe, the time-of-flight (TOF) system, the CsI(Tl) electromagnetic calorimeter (EMC), and the muon identifier (MU).

The time-of-flight system is based on a series of plastic scintillator bars that are read out by fine mesh photomultiplier tubes (PMT). It consists of a barrel and two end caps. The configurations of the barrel and end cap TOF are shown in Figs. 1 and 2 respectively. The barrel TOF has two layers of staggered scintillating bars mounted on the outer surface of the carbon fiber composite shell of the MDC, the radius of the inner layer barrel counters is 0.81 m. Each layer has 88 scintillator bars that are 2300 mm long and 50 mm thick with a trapezoidal cross-section. The two single layer end caps, each of which has 48 fan-shaped counters, are located outside the MDC end caps, 1330 mm away from the interaction point (IP) along the beam direction. The scintillator is 48 mm thick and 480 mm long. The inside end of the scintillator is cut at 45° to reflect light to the photomultiplier. The solid angle coverage of the barrel TOF is $|\cos\theta|<0.83$, while that of the end cap is $0.85<|\cos\theta|<0.95$.

Received 16 August 2013, Revised 27 September 2013

∗ Supported by Ministry of Science and Technology of China (2009CB825200) and National Natural Science Foundation of China (U1232201, 11121092, 11205180)

1) E-mail: zhangxj@ihep.ac.cn

2) E-mail: sunss@ihep.ac.cn

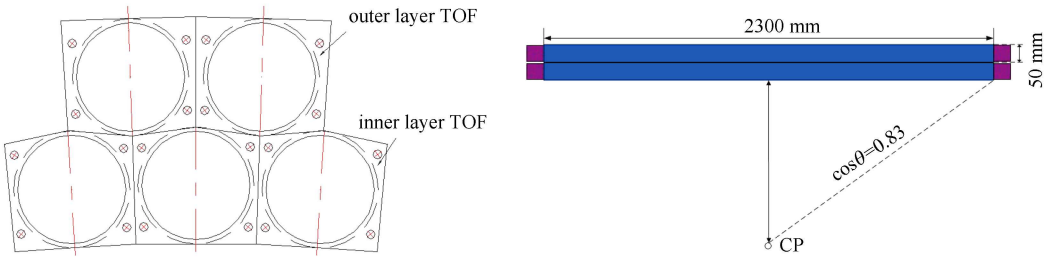


Fig. 1. Barrel TOF configuration.

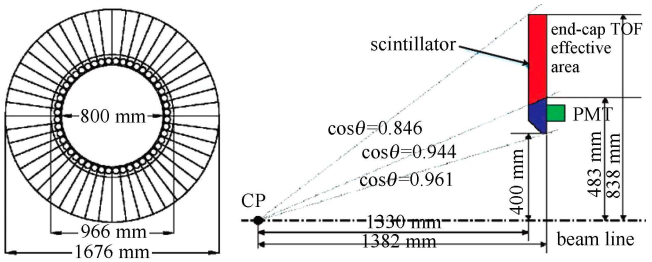


Fig. 2. End cap TOF configuration.

## 3 TOF simulation procedure

The exact description of the geometries and materials of the BESIII detector is implemented in the BES object-oriented simulation tool (BOOST) [6]. The hit information for incident particles passing through the scintillator is recorded in discrete steps, and both step size and energy loss are provided by GEANT4, depending on particle species and the characteristics of the current medium. Thus, the time of flight ($t_{\rm flight}$) and energy deposition in the scintillator can be obtained [7]. Optical photons are emitted isotropically from the point of energy deposition in the scintillator and they then propagate to the PMT located at the end of the scintillator. These physics processes, including Rayleigh scattering, medium-boundary interactions and absorption, are described using a parameterized simulation model instead of full GEANT4 simulation. This model is developed to meet the BESIII experiment's requirements for both accuracy and speed [8, 9]. The photon emission time, consisting of fast and slow components, is expressed as $t_{\rm emit}$, and the photon propagation time in the scintillator is expressed as $t_{\rm prop}$. When the photons arrive at a PMT photocathode, the photoelectrons produce an electric signal pulse according to the PMT response. The transit time of a single photoelectron signal in the PMT is defined as $t_{\rm transit}$. The PMT output pulse height is obtained by summing all the single photoelectron signals in the PMT,

$$V_{\rm PMT}(t)=\sum_{i=1}^{N_{\rm pe}} v_i(t), \tag{1}$$

where $v_i(t)$ is the signal from photoelectron $i$, and $N_{\rm pe}$ is the total number of photoelectron signals. The time $t$ at which a photoelectron arrives at the anode includes several components:

$$t=t_{\rm flight}+t_{\rm emit}+t_{\rm prop}+t_{\rm transit}. \tag{2}$$

Finally, the pulse is amplified by the preamplifier and discriminated by a double level threshold, and the charge and time information from a given channel are recorded. The signal time (TDC) is determined as the moment when the PMT pulse crosses the low-level threshold. For the charge, charge-to-time conversion ($QTC$) is the time integral of $V_{\rm PMT}(t)$ with the gain of the preamplifier $G_{\rm pre}$ and the resistance in the non-gated $QTC$ circuit $R_{\rm f}$:

$$QTC=\frac{\int G_{\rm pre}\cdot V_{\rm PMT}(t){\rm d}t}{R_{\rm f}}. \tag{3}$$

## 4 Monte Carlo tuning

### 4.1 Attenuation length and relative gain

Optical photons are propagated through total reflection, refraction and absorption in the scintillator. This effect is exponential with the effective attenuation length of the scintillator. The attenuation length of each counter is not necessarily the same, and is found to decrease with the aging effect. It is necessary to determine the attenuation length of each scintillator during a certain period of time from real data and to use these measured attenuation lengths as input parameters for the TOF simulation.

The gain of each PMT is different since it depends on the high voltage supply and the magnetic field intensity of its location. The factor of charge to voltage and the gain of the preamplifier are not uniform for each electronic readout channel. The relative gain for a given channel is used in Monte Carlo tuning to describe this difference.

For the barrel TOF, the observed pulse heights of two readout channels at two ends of a scintillator, $Q_1$ and $Q_2$, can be expressed as

$$\begin{aligned} Q_1 &= A_1 \cdot \frac{Q_0}{\sin\theta} \cdot \exp\left(-\frac{l/2-z}{L_{\rm atten}}\right), \\ Q_2 &= A_2 \cdot \frac{Q_0}{\sin\theta} \cdot \exp\left(-\frac{l/2+z}{L_{\rm atten}}\right), \end{aligned} \tag{4}$$

where subscripts 1 and 2 represent the readout channels in the direction along the $z$ axis and the opposite direction, respectively, $A_1$ and $A_2$ are the relative gains of the PMT and preamplifier for the two readout channels, $\theta$ is the polar angle of the incident particle with respect to the $z$ axis, $l$ is the total length of the scintillator bar, $z$ is the extrapolated hit position along the scintillator bar, $Q_0$ is the normalized pulse height at $z=0$ and $\theta=90^\circ$, and $L_{\rm atten}$ is the attenuation length of the scintillator. From Eq. (4), it is easily found that

$$\ln\left(\frac{Q_1}{Q_2}\right) = \ln\left(\frac{A_1}{A_2}\right) - \frac{2\cdot z}{L_{\rm atten}}. \tag{5}$$

The attenuation length $L_{\rm atten}$ and relative gain ratio $A_1/A_2$ can be obtained by doing a linear fit to $\ln(Q_1/Q_2)$ versus $z$ using real data. Then, the normalized pulse height can be expressed as:

$$Q_0 = \frac{\sin\theta}{A_2} \cdot \frac{Q_1 \cdot \exp\left(\frac{l/2-z}{L_{\rm atten}}\right) + Q_2 \cdot \exp\left(\frac{l/2+z}{L_{\rm atten}}\right)}{1+A_1/A_2}. \tag{6}$$

With the assumption that $Q_0$ for each counter has the same value, the relative gain $A_2$ of each readout channel can be normalized.

The attenuation lengths and relative gains are obtained using muons in dimuon events from real data because muons do not have hadronic interactions or large electromagnetic showers. These values are applied as input parameters for the TOF simulation. Using simulated dimuon events from the Monte Carlo sample, the attenuation lengths and relative gains are extracted using the same process as for real data. The distributions of attenuation length, relative gain ratio and normalized relative gain of data and Monte Carlo versus TOF counter number are shown in Figs. 3–5. The difference between data and Monte Carlo is defined as $(q_{\rm data}-q_{\rm MC})/q_{\rm data}$, where $q$ represents attenuation length, relative gain ratio or normalized relative gain. The differences are also shown in Figs. 3–5 with the vertical axis on the right side of the plots.

The pulse height measured by the TOF is used to determine the energy deposited in the scintillator in order to allow energy correction in the EMC reconstruction. The Monte Carlo tuning of attenuation length and relative gain is also helpful to improve the accuracy of the EMC simulation.

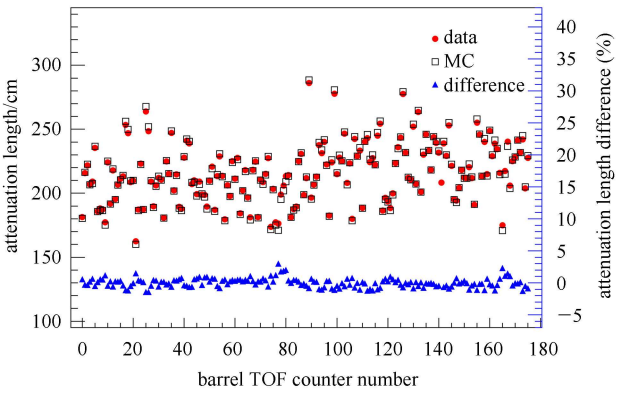


Fig. 3. Attenuation length of data and Monte Carlo, and difference versus TOF counter number.

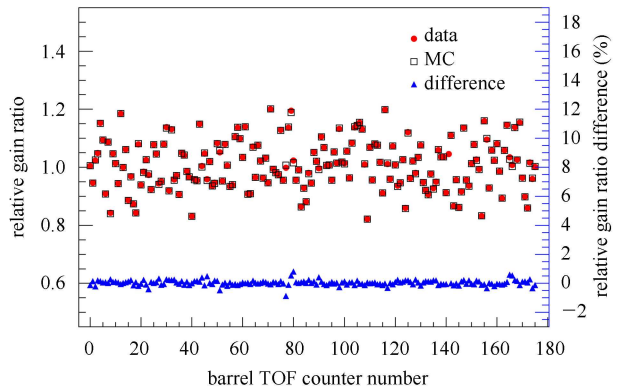


Fig. 4. Relative gain ratio of data and Monte Carlo, and difference versus TOF counter number.

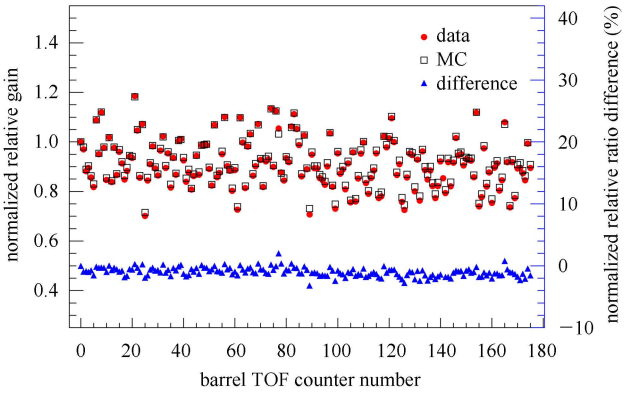


Fig. 5. Normalized relative gain of data and Monte Carlo, and difference versus TOF counter number.

### 4.2 The saturation effect

There is an obvious peak around channel 8200 in the distribution of pulse height for real data, which is shown as solid dots in Fig. 6, where 'channel' is the unit of measured pulse height, 1 channel representing 100 ps.

This unexpected peak is caused by a kind of saturation effect in the TOF readout electronics, where the signal is large enough to exceed the dynamic range. A sweep test of charge measurement has been performed by sending a group of same-shaped pulses with a programmable signal size from a pulse generator to the input of a front-end electronics module (FEE). The pulse shape is set by a PMT signal template acquired with a digital oscilloscope in a magnetic field. The sweep test result for a typical electronic readout channel is shown as hollow circles in Fig. 7, the $x$ and $y$ coordinates of each point representing the fixed value of input signal from the pulse generator and the measured pulse height of the electronic readout channel, respectively. The existence of an inflection point close to channel 8200 forms a peak with the accumulation of events, and the curve can be well described using a cubic polynomial in the dynamic range region [10]. The saturation curve of each electronic readout channel is obtained using the following function to fit the result of the sweep test:

$$f(x)=(a_0+a_1\cdot x+a_2\cdot x^2+a_3\cdot x^3)\cdot\left(1-\mathrm{erf}\left(\frac{x-a_4}{a_5}\right)\right)+(a_6+a_7\cdot x)\cdot\left(1+\mathrm{erf}\left(\frac{x-a_8}{a_9}\right)\right), \quad (7)$$

where $x$ is the value of input signal and $a_i$ ($i$=0, 1,$\cdots$,9) are parameters which are determined from fitting. As one of the important steps in TOF calibration, the time walk correction is used to remove the pulse height dependence of the measured time. This is sensitive to the precision of the measured pulse height, which is different for events within and in excess of the dynamic range. In the TOF simulation, the original pulse signal follows a Landau distribution, and the saturation peak is shaped by the pulse height distribution with the saturation curve given by Eq. (7) applied. The simulated pulse height distribution is shown as the histogram in Fig. 6.

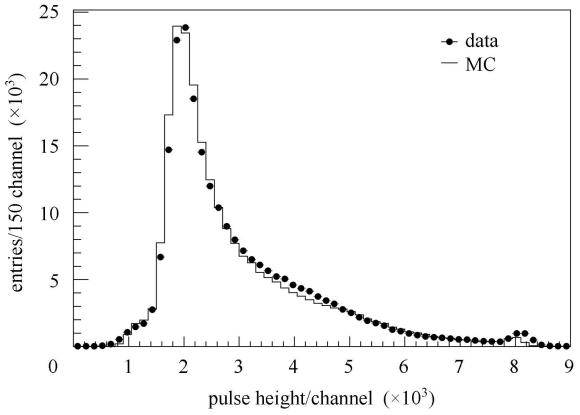


Fig. 6. The pulse height distribution of a typical channel.

The raw pulse height with saturation can be corrected in reconstruction using the inverse function of the saturation curve, with both real data and MC following the same process. The distributions of pulse height with saturation correction for barrel TOF and end cap TOF, for both data and MC, are shown in Fig. 8 and Fig. 9.

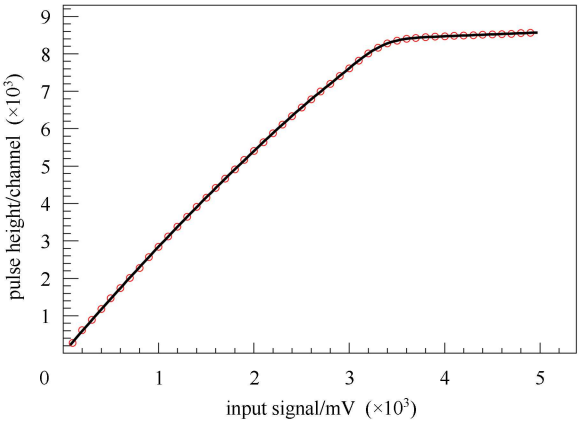


Fig. 7. The saturation curve of a typical channel.

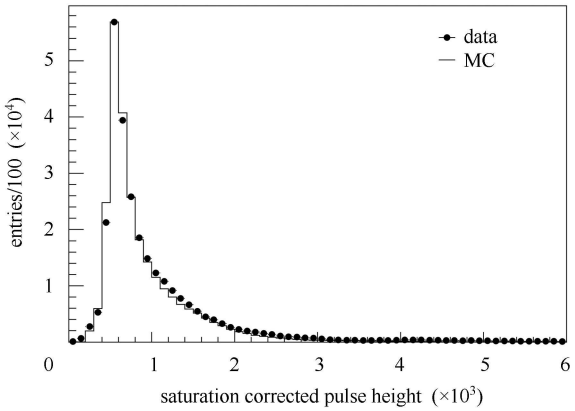


Fig. 8. Saturation corrected pulse height distribution for the barrel TOF.

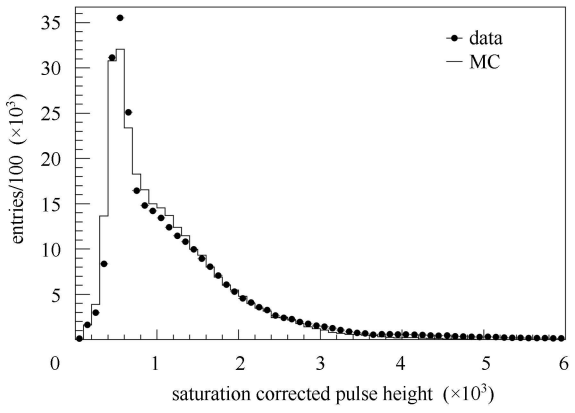


Fig. 9. Saturation corrected pulse height distribution for the end cap TOF.

### 4.3 Threshold and hit efficiency

When optical photons arrive at a PMT, an amplified signal pulse is produced and is discriminated by a double level threshold. The dual threshold discriminator scheme, which is designed to reduce noise while maintaining low time walk, is used for time digitization. The outputs from the low threshold discriminators are used to start the precision time-to-digital conversion (TDC) process and are put into coincidence with the high threshold discriminator outputs in order to reduce background rates. The signal time is then determined as the moment when the PMT pulse crosses the low-threshold, but only if the pulse height is larger than the high-level threshold. The same dual threshold method is followed for TOF simulation as for real data.

The TOF hit efficiency is defined as the number of charged tracks with a time difference less than 1.0 ns ($N_{|\Delta t|<1}$), to suppress the background, over the number of extrapolated tracks ($N_{\rm extrapolated}$):

$$\epsilon=\frac{N_{|\Delta t|<1}}{N_{\rm extrapolated}}. \tag{8}$$

The distribution of hit efficiency versus $z$ hit position of incident particles for data, using electrons in Bhabha events for one readout channel (east end) of the barrel TOF, is shown in Fig. 10. Fig. 11 shows the hit efficiency versus $r$ hit position for the end cap TOF. The differences between data and Monte Carlo for barrel and end cap TOF, defined as $(\epsilon_{\rm data}-\epsilon_{\rm MC})/\epsilon_{\rm data}$, are also shown in Figs. 10 and 11 with the vertical axis on the right side of the plots, respectively.

The observed pulse height follows an exponential trend, as given by Eq. (4), while the hit efficiency is reduced with increased distance between the hit position and the PMT. The energy deposited in a scintillator in response to the passage of charged particles also depends on the incident angle of the particle; that is, the effective distance traveled in passing through the scintillator. So, in the further part of the scintillator, the efficiency increases slightly with increased light propagation distance.

The high level threshold in the simulation has been tuned to make the efficiency consistent with that of data. The low level threshold has been tuned to retain the same ratio with the high level threshold as for real data. The TOF hit efficiency trend for MC is similar to that of the data.

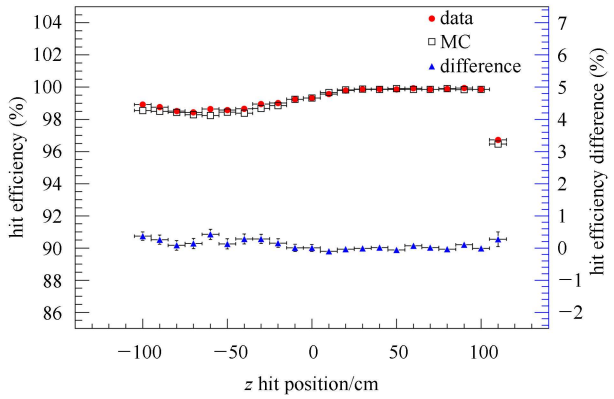


Fig. 10. Distribution of hit efficiency of data and Monte Carlo and difference versus hit position for barrel TOF.

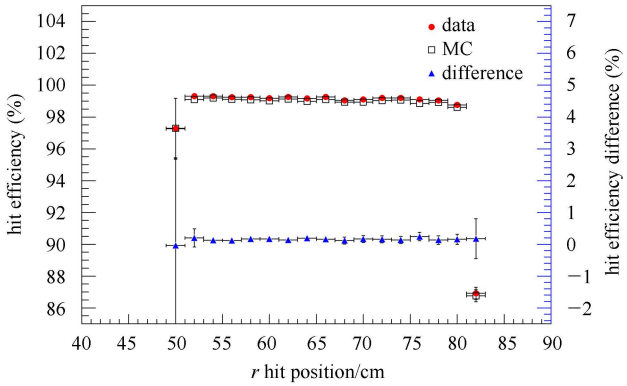


Fig. 11. Distribution of hit efficiency of data and Monte Carlo, and difference versus hit position for end cap TOF.

### 4.4 Time resolution

The time resolution of the TOF system is related to many variables, including the intrinsic resolution of the TOF, the uncertainties in the beam bunch time, beam bunch size, TOF electronics, extrapolated position, expected time of flight, and the uncertainty from the time walk effect.

$$\sigma=\sqrt{\sigma^2_{\rm intrinsic}+\sigma^2_{\rm bunchtime}+\sigma^2_{\rm bunchsize}+\sigma^2_{\rm electronics}+\sigma^2_{\rm extrapolate}+\sigma^2_{\rm expected}+\sigma^2_{\rm timewalk}}. \tag{9}$$

The "intrinsic" time resolution term $\sigma_{\rm intrinsic}$ is determined by the rise time of the scintillation light, the fluctuations of photon arrival time at the PMT, and the transit time spread of the PMT. The photon yield of the scintillator has been tuned, and the attenuation length is obtained from the real data. The time smear from the uncertainty of the PMT transit time is also considered in the simulation.

The bunch time term $\sigma_{\rm bunchtime}$ is mainly caused by the uncertainty in registering the global timing marker (accelerator RF clock) in the readout electronics, which is estimated to be about 20ps, including the jitter due to

the cables.

The uncertainty from the bunch size $\sigma_{\rm bunchsize}$ is caused by the uncertainties in determining the interaction points when two beam bunches of certain length collide. The bunch size varies during data taking, and mainly depends on the energy point. In our simulation the real bunch size acquired from data is used [11].

The uncertainty the from electronics $\sigma_{\rm electronics}$ mainly comes from the white noise of the electronics. This term has been tuned to around 20 ps to make the time resolution of MC consistent with that of the data. The uncertainties of the hit position along the scintillator bar $\sigma_{\rm extrapolate}$ and the expected time of flight $\sigma_{\rm expected}$ are determined by the MDC track reconstruction and extrapolation. These uncertainties are larger for the end cap counters than for the barrel counters because the charged particles that hit the end caps are tracked by fewer outer layers of the MDC.

The term $\sigma_{\rm timewalk}$ is the uncertainty caused by the time walk in a fixed threshold discriminator due to signal amplitude fluctuations. It should remain even when the electronics calibration is based on signal pulse height measurements.

Figure 12(a) and (b) shows the differences between the measured time and expected time for MC and data, and for the barrel and end cap TOF, respectively. The time resolutions for the barrel TOF are (66.5±0.1) ps and (67.7± 0.1) ps for data and Monte Carlo, respectively, and they are (152.1±0.3) ps and (155.1±0.3) ps for end cap TOF.

### 4.5 Dead channel and background simulation

A few of the TOF electronic readout channels have no signals during certain periods of data taking, which particularly affects the efficiency of offline data reconstruction. In the TOF simulation of the corresponding run numbers, the pulse height and time information are not produced for these dead channels in order to avoid introducing extra systematic error. The barrel TOF consists of two layers of scintillator bars read out by fine mesh photomultiplier tubes at both ends of the bars. There are usually four PMT readout signals for one charged particle passing through the two layers of the scintillator in the barrel TOF: one single dead channel will not have a significant impact on the reconstruction efficiency. The reconstructed time of flight is obtained as the weighted time of the layer that does not have the dead channel. For the end cap TOF, since there is only one readout channel per scintillator bar, the efficiency drops significantly if dead channels exist.

The beam background data acquired during data taking experiments, random triggers, is merged into the MC signals in the simulation.

During real data taking, a space electromagnetic effect that is related to the beam current is observed in the east end cap TOF for TOF counter numbers less than 48. The TOF signals are contaminated with this effect

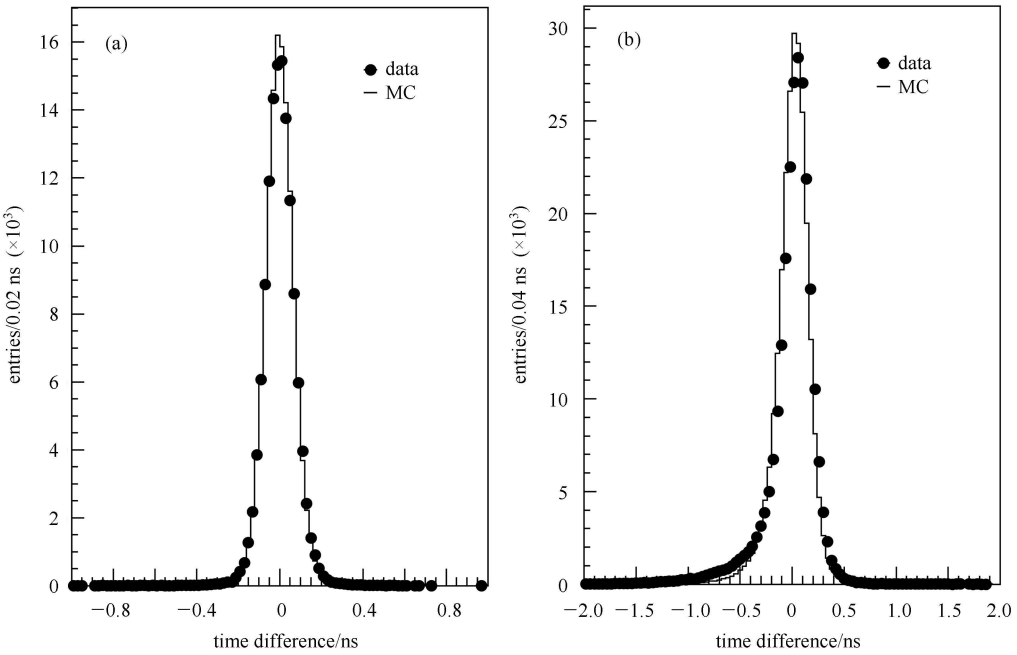


Fig. 12. Differences in measured time and expected time for barrel TOF (a) and end cap TOF (b). The solid dots are data and the hollow boxes are MC.

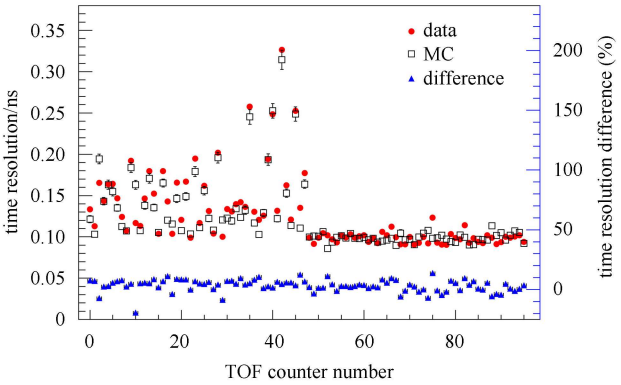


Fig. 13. Distribution of time resolution of data and Monte Carlo, and the difference versus TOF counter number for end cap TOF.

and the time resolutions become bad. Fig. 13 shows the distribution of time resolution versus TOF counter number. The bad time resolutions for some TOF counters indicate a high noise level. An extra term is added to the simulation of time resolution of each TOF counter in order to improve the consistency with the data. This gives an MC resolution similar to that of the real data, as shown in Fig. 13. The time resolution difference, which is defined as $(\sigma_{\rm data}-\sigma_{\rm MC})/\sigma_{\rm data}$ with $\sigma$ represents the time resolution, is also shown in Fig. 13, with the vertical axis on the right side of the plot.

## 5 Conclusion

A full simulation model for the BESIII TOF detector has been developed. Further Monte Carlo tuning of the detector characteristics has been applied for precise simulation of the physics processes. Using the attenuation lengths, relative gains, and saturation curves obtained from the real data, the pulse height is well simulated, and the dependence of hit efficiency on hit position is reproduced by tuning of the dual threshold discriminator. The MC tuning has improved the performance of the TOF system simulation, which is consistent with the real data. The TOF simulation is an important component of the BESIII MC that is used for physics analysis.

## References

1 BESIII collaboration. The Preliminary Design Report of the BES老贸 Detector. Beijing: IHEP-BEPCII-SB-13, 2004
2 Ablikim M et al. Nuclear Instruments and Methods in Physics Research A, 2010, **614**: 345–399
3 ZHANG C. for BEPC & BEPC Ⅱ Teams. Performance of the BEPC and progress of the BEPC Ⅱ. In: Proceedings of APAC. Gyeongju Korea, 2004, 15–19
4 Agostinelli S et al. GEANT4 Collab. Nucl. Instrum. Methods A, 2003, **506**: 250
5 Allison J et al. IEEE Trans. Nucl. Sci., 2006, **NS-53**: 270
6 DENG Z Y et al. High Energy Phys. Nucl. Phys., 2006, **30**: 371 (in Chinese)
7 LIU Y et al. Nuclear Instruments and Methods in Physics Research A, 2011, **629**: 87–92
8 DENG Zi-Yan. The Improvement and Upgrade of BESIII Offline Software (Postdoctor Research Report). Beijing: Institute of High Energy Physics, CAS, 2008 (in Chinese)
9 Nam J W et al. Nucl. Instrum Methods A, 2002, **491**: 54
10 ZHAO C et al. Chinese Physics C (HEP & NP), 2011, **35**: 72
11 XU M et al. Chinese Physics C (HEP & NP), 2010, **34**: 92